Ginsenosides alleviate the progression of hepatic fibrosis by targeting the liver circadian clock gene *CLOCK*

JIAWEN YU[1*], CHUNMEI QIAN[2*], RENYE QUE[1,3] and YI ZHOU[1]

[1]Department of Gastroenterology, Shanghai Municipal Hospital of Traditional Chinese Medicine, Shanghai University of Traditional Chinese Medicine, Shanghai 200071, P.R. China; [2]Science and Technology Innovation Center, Shanghai Municipal Hospital of Traditional Chinese Medicine, Shanghai University of Traditional Chinese Medicine, Shanghai 200071, P.R. China; [3]Department of Gastroenterology, Shanghai Traditional Chinese Medicine Integrated Hospital, Shanghai University of Traditional Chinese Medicine, Shanghai 200082, P.R. China

Received November 26, 2025; Accepted April 20, 2026

DOI: 10.3892/mmr.2026.13973

Abstract. Hepatic fibrosis (HF) serves as a critical pathological process underlying the progression of cirrhosis and hepatocellular carcinoma. Despite its clinical relevance, effective anti-fibrotic therapies remain scarce. Although total ginsenosides (GSS) can ameliorate hepatic oxidative damage and attenuate the development of HF, the molecular mechanism mediating their anti-fibrotic effects remains incompletely elucidated. Notably, circadian clock gene dysregulation is associated with hepatic metabolic dyshomeostasis and the fibrotic process. As a core circadian gene in the liver, clock circadian regulator (CLOCK) serves a role in the progression of fibrosis. The present study hypothesized that GSS may exert anti-fibrotic effects by restoring hepatic circadian rhythmicity through circadian clock-dependent pathways. Using a well-established carbon tetrachloride-induced murine model of HF in C57BL/6 mice, GSS was administered intraperitoneally at graded doses of 50, 100 and 200 mg/kg. Subsequently, serum and liver tissues were collected from mice for histopathological examination. Furthermore, the expression levels of fibrotic markers (α-smooth muscle actin and collagen type 1) and circadian rhythm genes [CLOCK, basic helix-loop-helix ARNT-like 1, cryptochrome (CRY)1, CRY2, period circadian protein homolog (PER)1 and PER2 were assessed. At the cellular level, LX-2 hepatic stellate cells (HSCs) were activated with TGF-β1 and treated with GSS, after which, RNA sequencing was performed on GSS-treated cells. In addition, the CLOCK inhibitor (CLK8) was used for *in vitro* experiments. The results of the present study revealed that GSS intervention effectively reversed the dysregulation of circadian gene expression and alleviated the progression of fibrosis. Molecular docking analysis further supported the interaction between GSS active components and the CLOCK protein. Thus, the current study focused on GSS and explored its role in ameliorating HF through regulation of the core circadian gene CLOCK. Collectively, the findings demonstrated that GSS may alleviate HF by rescuing circadian clock-driven circadian homeostasis in hepatocytes and HSCs, thereby providing mechanistic insight into traditional Chinese medicine-based interventions and identifying CLOCK as a druggable node for fibrosis therapy.

Introduction

Hepatic fibrosis (HF) represents a maladaptive wound-healing response triggered by recurrent hepatocyte injury, leading to excessive extracellular matrix (ECM) deposition and its aberrant distribution (1). This process is a universal feature of chronic liver diseases and constitutes the pivotal bridge linking persistent inflammation to cirrhosis and, ultimately, hepatocellular carcinoma (2). Given the decisive influence of HF on long-term prognosis, halting or reversing fibrogenesis is a therapeutic priority. Viral, parasitic, chemical, pharmaceutical, alcoholic and autoimmune insults can all incite necroinflammatory cascades that converge on hepatic stellate cell (HSC) activation, the central effector of ECM overproduction and progressive scarring (3). Consequently, beyond etiology-specific therapy, pharmacological reversal of fibrosis is now regarded as the cornerstone of chronic liver disease management. Substantial experimental evidence has confirmed that suppression of HSC activation markedly attenuates fibrotic progression (4).

The circadian clock is an evolutionarily conserved endogenous timing system that coordinates physiology, metabolism

Correspondence to: Dr Yi Zhou, Department of Gastroenterology, Shanghai Municipal Hospital of Traditional Chinese Medicine, Shanghai University of Traditional Chinese Medicine, 274 Zhijiang Middle Road, Shanghai 200071, P.R. China
E-mail: elian_zhou@163.com

Dr Renye Que, Department of Gastroenterology, Shanghai Traditional Chinese Medicine Integrated Hospital, Shanghai University of Traditional Chinese Medicine, 230 Baoding Road, Shanghai 200082, P.R. China
E-mail: 824492@qq.com

*Contributed equally

Key words: ginsenosides, circadian rhythm, *CLOCK* gene, hepatic fibrosis, hepatic stellate cells1

and behavior with the 24-h light/dark cycle (5). In mammals, the master pacemaker resides in the suprachiasmatic nuclei (SCN) of the hypothalamus. Light input via retinal photoreceptors entrains SCN neuronal oscillators and, in turn, aligns subsidiary clocks in virtually every peripheral tissue to the 24-h solar cycle (6). These peripheral oscillators operate autonomously in organs such as the liver, kidney, pancreas, skeletal and cardiac muscle; these peripheral clocks sustain rhythmic gene expression through transcriptional-translational feedback loops (7). Core components include the heterodimeric transcription factors clock circadian regulator (*CLOCK*) and basic helix-loop-helix ARNT-like 1 (*BMAL1*), the period circadian protein homolog (PER)1-3 and cryptochrome (CRY)1/2 proteins, and nuclear receptors such as Rev-Erbα. The hepatic clock integrates systemic cues with local metabolic demands (8). Its architecture comprises input pathways (9), a central oscillator (comprising a core loop and a stabilizing loop), and output arms that gate liver-specific rhythms (10). Disruption of this network has increasingly been recognized as a pathogenic driver of hepatitis (11), steatosis (12), fibrosis (13), cirrhosis (14) and hepatocellular carcinoma (15). As a basic helix-loop-helix-PER-ARNT-SIM transcription factor, *CLOCK* dimerizes with *BMAL1* to drive rhythmic expression of *CLOCK*-controlled genes governing metabolism, redox balance and cell proliferation (16). Rodent models bearing germline *CLOCK* mutations exhibit dampened circadian gene expression, metabolic syndrome, cognitive deficits and multi-organ pathology, including accelerated HF, highlighting the non-redundant role of *CLOCK* in hepatic homeostasis (17). Similarly, genetic ablation of *PER1/2* or *BMAL1* perturbs hepatic circadian function, resulting in systemic metabolic disturbances, including fasting hyperglycemia, hyperlipidemia, hepatomegaly, and progressive liver pathology characterized by cholangiocyte hyperplasia, chronic inflammation, hepatocyte apoptosis and collagen deposition (18).

Ginsenosides (GSS) are a standardized saponin-rich extract predominantly derived from the roots of *Panax ginseng* (19), and represent one of the most pharmacologically important bioactive fractions of this medicinal herb. The synergistic actions of these compounds underlie a number of documented physiological effects, including immunomodulation, anti-fatigue activity, neuroprotection, glucose and blood pressure homeostasis, and potent antioxidant capacity. Among these properties, the anti-fibrotic potential of individual GSS has received notable attention; for example, Rg3 (20) suppresses HSC activation and inflammatory cascades (21), whereas Rg1 activates the Nrf2-ARE pathway to counteract oxidative stress-driven ECM accumulation (22). Building on this foundation, the present study aimed to systematically evaluate the therapeutic impact of GSS in carbon tetrachloride (CCl_4)-provoked murine fibrosis and in TGF-β1-challenged LX-2 cells, while assessing the functional involvement of the core circadian transcription factor *CLOCK* in the fibrotic program, thereby defining a previously uncharacterized chronotherapeutic axis in fibrosis suppression.

Materials and methods

Chemicals and reagents. GSS was purchased from Shanghai Yuanye Bio-Technology Co., Ltd. (UV ≥80%) (23). CCl_4 solution was obtained from Sinopharm Chemical Reagent Co., Ltd. Olive oil was sourced from MilliporeSigma. Human TGF-β1 Recombinant Protein was purchased from Wuhan Sanying Biotechnology. The selective CLOCK inhibitor (CLK8) was purchased from MedChemExpress.

Animals. A total of 60 male C57BL/6 mice (age, 6-8 weeks; weight, 18-22 g) were purchased from Shanghai Model Organisms Center, Inc. The mice were acclimated under specific pathogen-free conditions at Shanghai Hospital of Traditional Chinese Medicine (Shanghai, China) under the following conditions: Adaptation period of 1 week, ambient temperature maintained at 20-25˚C, humidity at 40-70%, 12-h light/dark cycle, quiet environment, and free access to food and water. All procedures conformed to National Standards for Laboratory Animals of China and were approved by the Animal Ethics and Welfare Committee of Shanghai Municipal Hospital of Traditional Chinese Medicine (ethics approval no. 2025051; Shanghai, China).

The mice were randomly assigned to six groups (n=10/group): i) Control group (vehicle only), ii) CCl_4 model group, iii) GSS low-dose group (50 mg/kg), iv) GSS medium-dose group (100 mg/kg), v) GSS high-dose group (200 mg/kg) and vi) resveratrol(Macklin Inc.) positive control group (30 mg/kg). Based on the preliminary experimental foundation of our research group, the present study established three gradient doses (low, medium and high) encompassing the effective concentrations of GSS, aiming to comprehensively evaluate its dose-dependent effects. HF was induced by intraperitoneal injection of 20% CCl_4 in olive oil (v/v) twice weekly for 8 weeks in all groups except for the control group. The control group received equivalent volumes of olive oil on the same schedule. The GSS low, medium and high dose groups were administered GSS via intraperitoneal injection once daily for 4 weeks. The positive control group received resveratrol diluted in normal saline to a final concentration of 30 mg/kg via intraperitoneal injection once daily for 4 weeks.

Cell culture and treatment. LX-2 human HSCs were purchased from Shanghai Zhong Qiao Xin Zhou Biotechnology. Cells were maintained at 37˚C in a 5% CO_2 incubator using high-glucose DMEM (Gibco; Thermo Fisher Scientific, Inc.) supplemented with 10% fetal bovine serum (Shanghai Yeasen Biotechnology Co., Ltd.). For experiments, LX-2 cells were seeded into 6-well plates at a density of $3x10^5$ well and allowed to adhere overnight; they were then divided into the following sixdi) Control (untreated; 37˚C), ii) TGF-β1 (10 μg/ml; 6 h; 37˚C), iii) TGF-β1 + GSS (10 μg/ml TGF-β1 for 6 h followed by 1 mg/ml GSS for 24 h; 37˚C), iv) CLK8 (5 μM; 12 h; 37˚C), v) CLK8 + TGF-β1 (10 μg/ml TGF-β1 for 6 h followed by 5 μM for 12 h; 37˚C), vi) TGF-β1 + GSS + CLK8 (10 μg/ml TGF-β1 for 6 h; then 1 mg/ml GSS for 24 h; followed by 5 μM CLK8 for 12 h; 37˚C). At the same time, to investigate cell activation conditions, activation was modeled by treating HSCs with TGF-β1, TGF-β1 was administered at concentrations of 0, 5, 10, 20 and 40 μg/ml and treated for 0, 6, 12 and 24 h.

Measurement of serum levels of alanine aminotransferase (ALT), aspartate aminotransferase (AST), alkaline phosphatase (ALP), lactate dehydrogenase (LDH), laminin (LN), hyaluronan (HA), Procollagen type III (PC III) and Procollagen type IV (PC IV). At the end of the 8-week

experimental period, mouse blood sampling was performed via retro-orbital bleeding. Each mouse was subjected to blood collection (~0.2 ml), with the collected volume not exceeding 20% of the total blood volume. The maximum single blood collection volume was ~0.25 ml, as the total blood volume of a 30 g mouse is ~1.5 ml. Anesthesia was induced by intraperitoneal injection of 1% pentobarbital sodium (45 mg/kg), corresponding to an injection volume of ~0.135 ml/30 g mouse. Immediately after blood collection, sterile cotton balls were used to achieve hemostasis by compression and antibiotic ophthalmic ointment was applied. Subsequently, the mice were administered a pentobarbital sodium (90 mg/kg) and euthanized by cervical dislocation. The humane endpoints included body weight loss >20% of the initial body weight, inability to consume food and water by themselves, no mice required early euthanasia in the study. The blood samples were kept undisturbed and allowed to clot at room temperature for 30 min and centrifuged at 3,500 x g for 10 min at 4˚C. Serum was then aliquoted and stored at -20˚C for subsequent analysis. Commercially available assay kits were used to measure the serum levels of ALT (cat. no. BY-BC-K021), AST (cat. no. BY-BC-K022), LDH (cat. no. BY-BC-K045) and ALP (cat. no. BY-BC-K091) (Shanghai Baipu Biotechnology Co., Ltd.), and the serum levels of LN (cat. no. BY-EM220216), HA (cat. no. BY-WJZF0179), PC III (cat. no. BY-EM220067) and PC IV(cat. no. BY-EM228277) were quantified using ELISA kits (Shanghai Baipu Biotechnology Co., Ltd.). All kits were used strictly according to the manufacturers' protocols.

Histopathological examination. At the end of the 8-week experimental period, the mice euthanized by cervical dislocation and tissues were harvested from all liver lobes. The tissues were fixed in 4% paraformaldehyde at room temperature for 24 h and paraffin-embedded sections were prepared using conventional methods with a thickness of 5 μm. The sections were then stained with hematoxylin and eosin (H&E), Masson's trichrome and Sirius red dyes following standard protocols: for H&E staining, the sections were stained with 0.5% hematoxylin at room temperature (25±2˚C) for 5 min, followed by differentiation and counterstaining with 0.5% eosin at room temperature for 3 min. For Masson's trichrome staining, the sections were stained with 0.1% hematoxylin at room temperature for 8 min, followed by staining with 0.5% Masson's trichrome dye at room temperature for 15 min. for Sirius red staining, the sections were stained with 0.1% Sirius red dye at room temperature for 30 min. After staining, all sections were observed for pathological alterations and the degree of HF under a light microscope. The stained areas were semi-quantitatively analyzed using ImagePro Plus software (version 5.1; Media Cybernetics, Inc.).

Immunohistochemical staining. Liver tissue samples from mice were fixed in 4% paraformaldehyde at 4˚C for 24 h and routinely processed into paraffin-embedded sections with a thickness of 5 μm. The sections were first dewaxed with xylene (washing reagent) for 5 min twice, followed by rehydration in a descending alcohol series (100% ethanol for 3 min; 95% ethanol for 3 min; 80% ethanol for 3 min; 70% ethanol for 3 min) and rinsed with distilled water. For antigen retrieval, the sections were immersed in citrate buffer (pH 6.0) and heated in a water bath at 95-8˚C for 20 min, then cooled to room temperature naturally. Since the target antigens were intracellular antigens, permeabilization was performed with 0.1% Triton X-100 (permeabilization reagent) at room temperature for 10 min. Endogenous peroxidase activity was quenched with 3% hydrogen peroxide in methanol for 10 min at room temperature. Subsequently, the sections were blocked with 10% normal goat serum (Beijing Solarbio Science & Technology Co., Ltd.) at room temperature (25±2˚C) for 30 min, then incubated overnight at 4˚C with primary antibodies diluted in antibody diluent containing 1% BSA (MilliSigma). Subsequently, HRP-conjugated goat anti-rabbit IgG secondary antibodies were applied at a dilution of 1:500 and incubated at room temperature for 1 h. After chromogenic development and counterstaining, the sections were mounted with neutral balsam, avoiding bubble formation and observed under a microscope for imaging.

Triple immunofluorescence staining. LX-2 cells were seeded on glass coverslips at a cell density of $5x10^3$ cells and fixed with 4% paraformaldehyde in PBS for 10 min at room temperature, permeabilized with 0.1% Triton X-100 (or 0.2% Tween-20) for 10 min at room temperature, and blocked with 5% BSA + 0.1% Tween-20 at room temperature (25±2˚C) for 15 min. The cells were sequentially incubated with primary antibodies against CLOCK (1:500; cat. no. 18094-1; Proteintech Group, Inc.), BMAL1 (1:500; cat. no. ab230822; Abcam) and CRY2 (1:500; cat. no. 13997-1; Proteintech Group, Inc.) at 4˚C overnight. After washing with PBS, the cells were incubated with fluorescent-conjugated goat anti-rabbit IgG secondary antibodies (1:500; cat. no. ab150077; Abcam) for 1 h at room temperature. HRP-conjugated secondary antibodies are not suitable for immunofluorescence analysis (HRP is mainly used for chromogenic reactions in immunohistochemistry), so fluorescent-conjugated secondary antibodies were specifically used in this experiment to ensure the accuracy and reliability of fluorescence imaging results. Nuclei were stained with 1 μg/ml DAPI for 5 min at room temperature and washed with PBS. Finally, the samples were mounted with anti-fade mounting medium and imaged under a confocal microscope.

Western blotting. Briefly ~100 mg snap-frozen liver tissue/sample was homogenized in lysis buffer (cat. no. P0013B; Beyotime Biotechnology) for thorough grinding and complete lysis. For protein extraction from cells, the cells were washed twice with pre-cooled PBS, then lysed with the same lysis buffer (cat. no. P0013B; Beyotime Biotechnology) on ice for 30 min, followed by centrifugation at 12,000 x g for 15 min at 4˚C to collect the supernatant (total cellular protein). Protein quantification was performed using the BCA assay kit (cat. no. P0012; Beyotime Biotechnology) and the protein concentration of each sample was calculated for subsequent sample preparation. A total of 20 μg of protein per lane was loaded for electrophoresis. The PAGE gel was prepared using the Epizyme Fast PAGE Gel Preparation Kit (Ipsen Pharma) according to the manufacturer's instructions. Subsequent steps included electrophoresis, transfer onto a PVDF membrane (polyvinylidene fluoride membrane), blocking with 5% BSA at room temperature (25±2˚C) for 1 h, followed by overnight

Table I. Primer sequences used for reverse transcription-quantitative PCR.

Gene	Forward (5'-3')	Reverse (5'-3')
Human		
ACTIN (ACTB)	CCACCATGTACCCTGGCATT	GTCCTCGGCCACATTGTGAA
CLOCK	GATCACAGCCCAACCCCTTC	CTGGGTGGAGTGCTCGTATC
BMAL1	ACTGTGCTAAGGATGGCTGT	GCTGCCCTGAGAATGAGGTG
CRY1	CCTGGAATGCACCAGAAGGT	TCCACTGCTGCTACAACCTG
CRY2	CCAGCCAGGGAAACCATTCT	CTCTGGGTCAAACCTCCCAC
PER1	GACCCCTCATGCTGGCTATC	ACAGAAGCGGATAGGGGAGT
ACTA2d	AAAAGACAGCTACGTGGGTGA	GCCATGTTCTATCGGGTACTTC
COL1A1	TCTGGAGCAAGTGGTGAACG	CCCCTCACGTCCAGATTCAC
Mouse		
ACTIN	TGAGCTGCGTTTTACACCCT	TTTGGGGGATGTTTGCTCCA
CLOCK	CATCAACTCAGCAGAGTCAACA	AGGCTGGGAAATCACCATCG
BMAL1	AAAGATGGGGCTGGACGAAG	ACCCGTATTTCCCCGTTCAC
CRY2	TGGACAAGCACTTGGAACGGAAG	GTAGAAGAGGCGGCAGGAGAGG
α-SMA	GTCCCAGACATCAGGGAGTAA	CGGATACTTCAGCGTCAGGA
COL1A1	GAGACAGGCGAACAAGGTGA	GGGAGACCGTTGAGTCCATC

α-SMA, α-smooth muscle actin; *BMAL1*, basic helix-loop-helix ARNT-like 1; *COL1A1*, collagen type I α1; *CLOCK*, clock circadian regulator; *CRY*, cryptochrome; *PER1*, period circadian protein homolog 1.

incubation at 4˚C with the following primary antibodies: Anti-α-smooth muscle actin (α-SMA; cat. no. 19245; Cell Signaling Technology, Inc.), anti-collagen type 1 (COL-1; cat. no. 67288; Proteintech Group, Inc.), anti-CLOCK (cat. no. 18094-1-AP; Proteintech Group, Inc.), anti-BMAL1 (cat. no. ab230822; Abcam), anti-CRY1 (cat. no. ab54649; Abcam), anti-CRY2 (cat. no. 13997-1-AP; Proteintech Group, Inc.), anti-PER1 (cat. no. 13463-1-AP; Proteintech Group, Inc.; all 1:1,000). In addition, the membranes were incubated for 1 h at room temperature with anti-GAPDH (1:10,000; cat. no. 10494-1-AP; Proteintech Group, Inc.). Finally, the membranes were developed using the ECL chemiluminescence visualization reagent (cat. no. P0018M; Beyotime Biotechnology), and grayscale analysis of the bands was performed using ImageJ software (version 1.8.0_172; National Institutes of Health).

Reverse transcription-quantitative PCR (RT-qPCR). Total RNA was extracted from mouse liver tissues and LX-2 cells using the EZ-press RNA Purification Kit (cat. no. B004DP; EZBioscience) according to the manufacturer's instructions. No additional reagents or additives were used during RNA extraction with the EZ-press RNA Purification Kit from EZBioscience. RNA concentration and purity were measured with a NanoDrop 2000 instrument (NanoDrop; Thermo Fisher Scientific, Inc.). cDNA was synthesized in a 20-μl RT reaction system using the ChamQ RT Master Mix (cat. no. Q311-02; Vazyme Biotech Co., Ltd.). The temperature protocol for RT was as follows: 42˚C for 15 min (cDNA synthesis) and 85˚C for 5 sec (reverse transcriptase inactivation). qPCR amplification was performed using ChamQ Universal SYBR qPCR Master Mix (Vazyme Biotech Co., Ltd.) under the following cycling conditions: Amplification: 95˚C for 5 min, followed by 40 cycles at 95˚C for 10 sec and 60˚C for 30 sec; dissociation curve: 95˚C for 15 sec, 60˚C for 1 min and 95˚C for 30 sec. The $2^{-\Delta\Delta Cq}$ method was used for the quantification of target gene expression (24). We confirm that the primer sequences for all target genes and internal reference gene are accurately listed in Table I.

Transcriptome sequencing. Total RNA was isolated from LX-2 cells using the RNeasy Mini Kit (Cat. no. 74104; Qiagen), followed by on-column DNase digestion and eukaryotic mRNA was enriched using magnetic beads with Oligo (dT) included in the NEBNext Ultra RNA Library Prep Kit for Illumina (cat no. E7530L; New England BioLabs, Inc.). For prokaryotic samples, prokaryotic ribosomal RNA (rRNA) was removed using the Ribo-Zero rRNA Removal Kit (Bacteria) (cat. no. MRZB12424, Illumina, Inc.) to enrich mRNA). Fragmentation reagents were added to decompose the mRNA into small fragments, and these cleaved mRNAs were used as a template for first-strand cDNA synthesis with random hexamer primers. Subsequently, a second-strand synthesis reaction system was used to produce double-stranded cDNA, which was purified using the purification module included in the NEBNext library preparation kit. The purified double-stranded cDNA was subjected to end repair, A-tailing and adapter ligation. Subsequently, size selection was performed, followed by PCR amplification. The quality and integrity of the final sequencing library were verified using the Agilent 2100 Bioanalyzer (Agilent Technologies, Inc.) to confirm the fragment size distribution and library quality. The quantified library was normalized to a loading concentration of 2 nM, and sequenced on the Illumina HiSeq X-ten platform (Illumina, Inc.). The sequencing was performed in paired-end mode, with a read length of 150 bp for each end. To ensure the quality of

the data, before performing bioinformatics analyses, FASTQC (http://www.bioinformatics.babraham.ac.uk/projects/fastqc/) was used to evaluate the raw data, and poor quality data at the first reading were eliminated by pre-processing. Analyses were then performed, including gene expression determination, gene structure refinement, variable splice detection, identification of new transcripts, coding potential prediction and single nucleotide polymorphism detection. Specifically, clean reads were aligned to the reference genome using HISAT2 (v2.2.1; https://ccb.jhu.edu/software/hisat2/index.shtml), and transcript assembly and expression quantification were performed using StringTie (v2.2.1; https://ccb.jhu.edu/software/stringtie/). Differently expressed genes (DEGs) between the treatment and control groups of LX-2 cell samples were identified from the gene expression results. Genes with $|\log_2$ fold change$|\geq 1$ and Benjamini-Hochberg-adjusted P-value (false discovery rate) <0.05 were considered statistically significant. Based on these DEGs, cluster analysis, Gene Ontology (GO) functional enrichment analysis and pathway enrichment analysis were performed. A negative binomial distribution test was used to assess the significance of differences between readings and counts, and the baseline mean was used to estimate the level of gene expression.

Molecular docking analysis. To investigate the binding potential between the active ingredients of GSS and the core target CLOCK protein, molecular docking analysis was performed following a standard protocol. Briefly, 8 major active ingredients of GSS, including MC, Rb1, Rb2, Rg1, Rg3, Rg5, Rh1 and Rh2, were selected as the docking ligands based on our component characterization results. The 2D structural files of these small-molecule ligands were downloaded from the PubChem database (https://pubchem.ncbi.nlm.nih.gov/). Subsequently, the 2D structures were converted to optimized 3D structures, and the protonation state of each ligand was adjusted and optimized using OpenBabel (version 3.1.1; https://openbabel.org/). For the target protein preparation, the crystal structure of the human CLOCK protein was downloaded from the RCSB Protein Data Bank (PDB ID: 4h10; https://www.rcsb.org/), which was preprocessed to remove redundant water molecules and heteroatoms before docking. The protein-ligand blind docking was performed using the CB-Dock2 web server (version 1.0; https://cadd.labshare.cn/cb-dock2/), a comprehensive online tool that integrates structure-based docking and template-based docking to improve the accuracy of binding site prediction and binding conformation prediction. Default parameters of the web server were adopted for the whole docking analysis. After the docking calculation, the binding affinities of each ligand with the CLOCK protein were calculated via the built-in AutoDock Vina scoring function, with the unit of kcal/mol. Finally, the docking results were visualized using PyMOL software (version 2.5.0; Schrödinger, LLC; https://pymol.org/2/), to generate the protein-ligand interaction diagrams and binding heatmap.

Statistical analysis. All experiments were independently repeated at least three times with consistent results, and all statistical analyses were performed based on the biological replicates. Experimental data were analyzed using ImageJ and GraphPad Prism 9.0 (Dotmatics), and are presented as the mean ± SD. For normally distributed data, significant differences were determined by t-test (for comparisons between two groups) or one-way analysis of variance with Tukey's test (for comparisons among multiple groups). $P<0.05$ was considered to indicate a statistically significant difference.

Results

GSS improves liver function and HF in a CCl_4-induced model. A murine model of HF was established by induction with CCl_4 to evaluate the extent of liver injury and fibrosis, as well as the reversive effect of GSS treatment. GSS was administered at gradient concentrations to establish the dose-response relationship and to determine the optimal therapeutic dosage. In addition, resveratrol was selected as the positive control drug based on our preliminary findings, aiming to validate the successful establishment of the experimental model and enhance the credibility of the results. After 8 weeks, liver tissue samples were collected for histopathological examination using H&E, Masson's trichrome and Sirius red staining. After GSS administration, these pathological and biochemical abnormalities were markedly ameliorated in a concentration-dependent manner. Low-dose GSS partially alleviated inflammatory infiltration and reduced collagen deposition by ~25%. Medium-dose GSS achieved more prominent therapeutic effects, with obviously recovered hepatocellular structure, 50% reduction in fibrotic area. Notably, high-dose GSS exhibited a robust hepatoprotective and anti-fibrotic effect, which was comparable to that of the positive control resveratrol, the liver lobular structure was nearly restored to normal, the collagen deposition was largely resolved with only mild residual fibrosis (Fig. 1A). Serum levels of hepatic function and fibrosis markers were also measured, including AST, ALT, ALP, LDH, HA, LA, PC III and PC IV. Low-dose GSS accompanied by a mild reduction in serum injury and fibrosis markers. Medium-dose GSS significantly downregulated serum biomarker levels. Notably, the serum levels of all detected hepatic function and fibrosis markers were significantly reversed in high-dose GSS, close to the levels of the normal control group (Fig. 1B). The results demonstrated that GSS effectively attenuated hepatic inflammation, improved liver function and ameliorated HF in model mice in a concentration-dependent manner, exhibiting notable hepatoprotective effects.

GSS reverses CCl_4-induced expression of α-SMA and COL-1 in model mice. α-SMA and COL-1, key indicators of HF, were examined in the present study, since α-SMA serves as a marker of activated HSCs (25) and COL-1 is a major component of the ECM; elevated expression of both is closely associated with fibrosis progression. Therefore, immunohistochemical analysis (Fig. 2A), western blotting (Fig. 2B and C) and RT-qPCR (Fig. 2D) were performed on liver tissues to assess the protein and mRNA expression levels of α-SMA and COL-1. The CCl_4-treated group exhibited increased protein and mRNA expression levels of α-SMA and COL-1, whereas intervention with different concentrations of GSS exhibited a dose-dependent reduction on the expression levels of α-SMA and COL-1. Notably, high concentrations of GSS and treatment with resveratrol demonstrated the strongest antifibrotic effect.

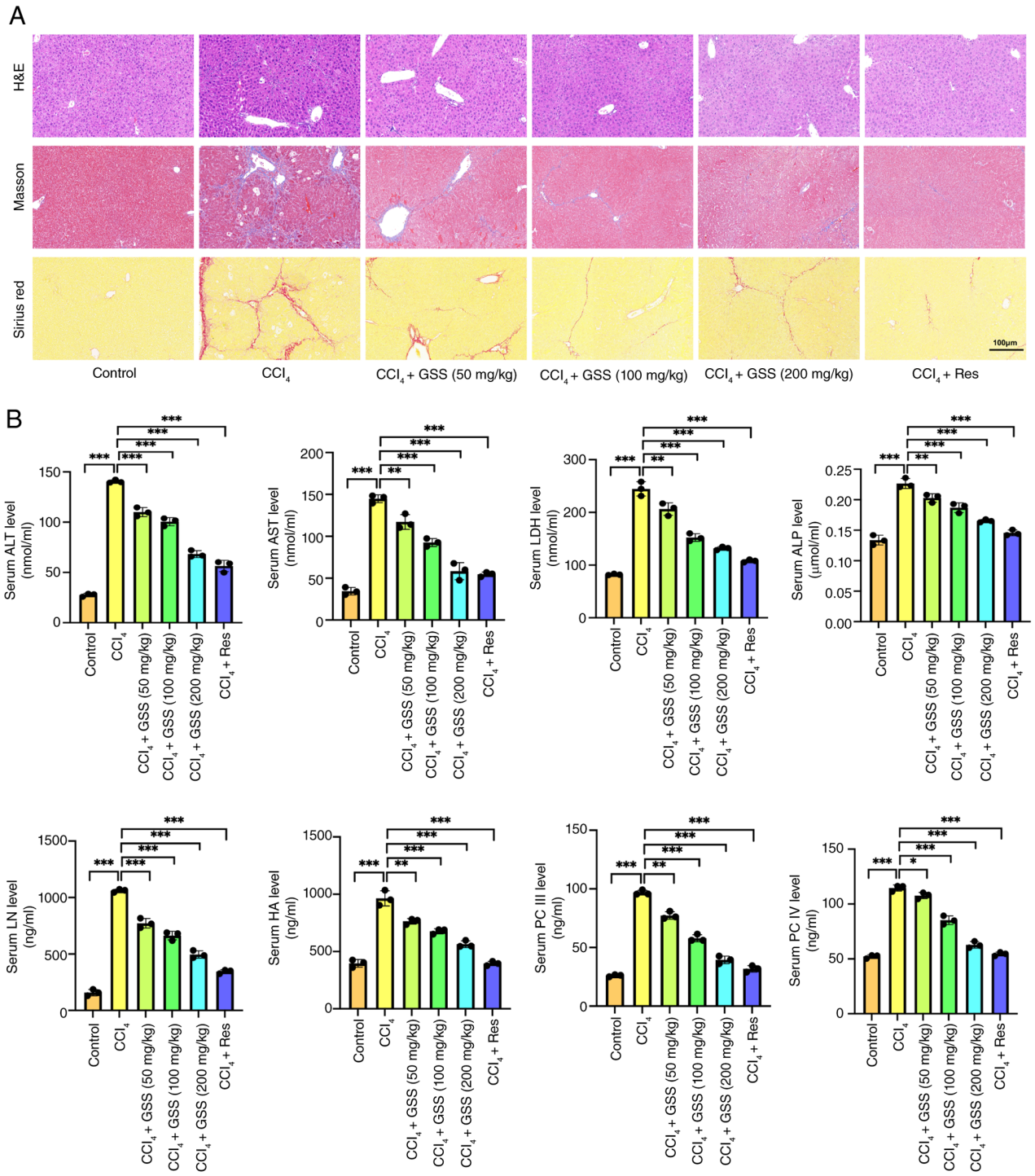

Figure 1. GSS improves liver function and hepatic fibrosis levels in CCl_4-induced modeling. GSS alleviated the progression of liver fibrosis in mice with CCl_4-induced modeling. (A) Histological examination of mouse liver tissues. (B) Serum parameters of liver function and fibrosis in mice. Compared with the control group (within the normal range of serum levels), the serum levels of liver function and hepatic fibrosis indices were significantly elevated in the model group mice, while the ginsenoside group dose-dependently reversed the serum levels of liver function and hepatic fibrosis in mice. Data are presented as the mean ± SD from three independent replicates. *P<0.05, **P<0.01, ***P<0.001. ALP, alkaline phosphatase; PC, procollagen; ALT, alanine aminotransferase; AST, aspartate aminotransferase; CCl_4, carbon tetrachloride; GSS, ginsenosides; H&E, hematoxylin and eosin; HA, hyaluronan; LDH, lactate dehydrogenase; LN, laminin; Res, resveratrol.

These results indicated that CCl_4 resulted in notable progression of HF, whereas GSS effectively inhibited the development of fibrosis.

GSS suppresses TGF-β1-induced activation of HSCs. HSC activation is a critical driver of HF; the process begins with HSC transformation into myofibroblasts, a key event leading to ECM deposition and liver damage (4). To investigate this, activation was modeled by treating HSCs with TGF-β1, and monitoring α-SMA and COL-1 expression. TGF-β1 was administered at concentrations of 0, 5, 10, 20 and 40 μg/ml (Fig. 3A and B), and the optimal concentration of 10 μg/ml was

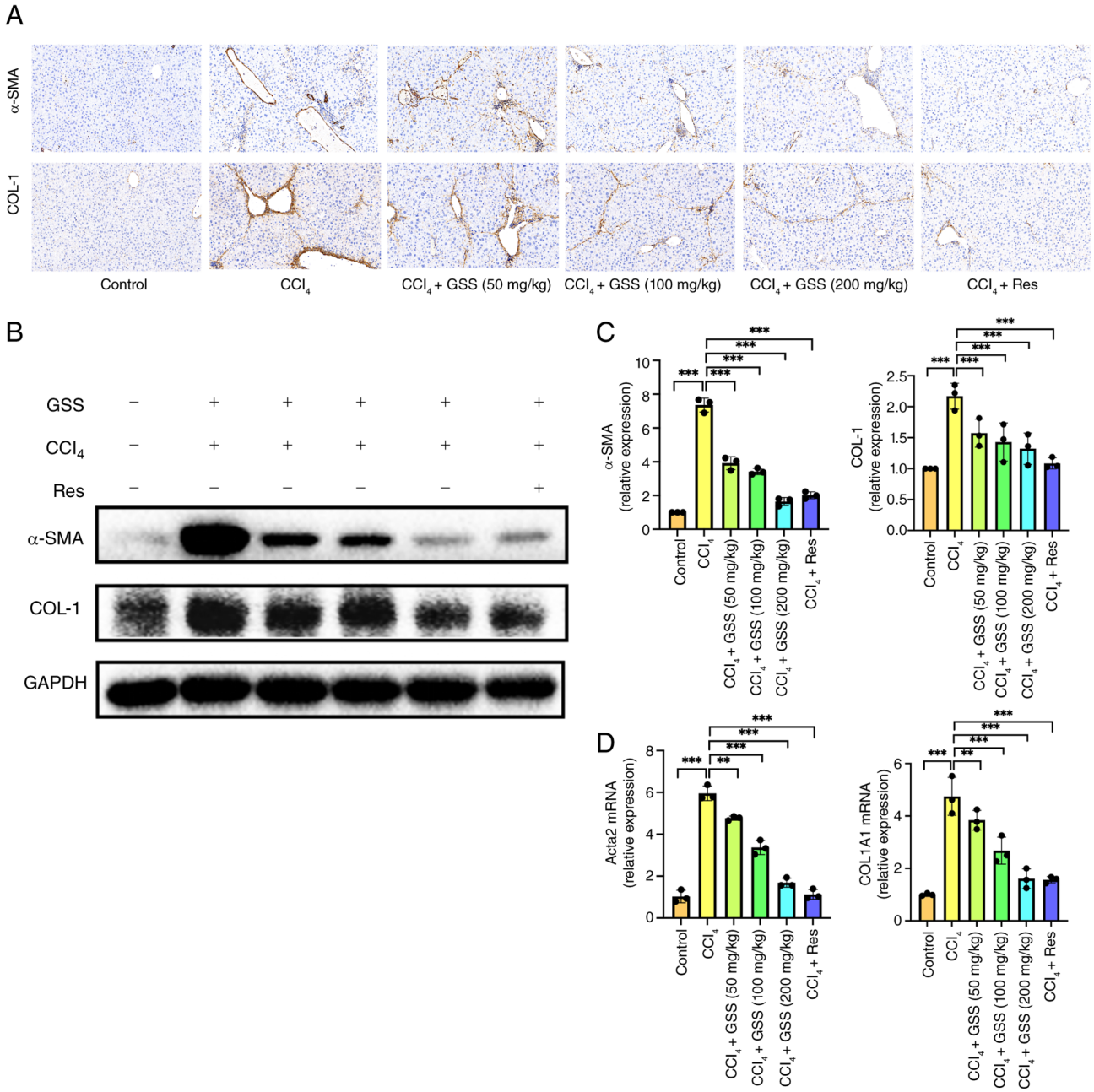

Figure 2. GSS reverses CCl_4-induced expression of α-SMA and COL-1 in model mice. (A) Immunohistochemical analysis of mouse liver tissues. (B) Western blot analysis of α-SMA and COL-1 expression. (C) Protein expression levels of α-SMA and COL-1. (D) mRNA expression levels of α-SMA and COL-1. Compared with the control group, the protein and mRNA expression levels of α-SMA and COL-1 in the liver tissues of CCl_4 model mice were significantly increased and ginsenoside intervention reversed their expression in a dose-dependent manner. Data are presented as the mean ± SD from three independent replicates. **P<0.01, ***P<0.001. α-SMA, α-smooth muscle actin; CCl_4, carbon tetrachloride; COL-1, collagen type 1; GSS, ginsenosides; Res, resveratrol.

used to stimulate HSCs for 0, 6, 12 and 24 h (Fig. 3C and D). The results showed that TGF-β1 at 10 μg/ml induced maximum activation of HSCs after 6 h of stimulation, with significant pro-fibrotic effects observed. Under these conditions, HSCs were markedly activated, and the protein and mRNA expression levels of α-SMA and COL-1 were considerably increased. This effect was effectively reversed by GSS treatment (Fig. 3E-G).

Investigation of the targets underlying the anti-fibrotic effects of GSS. To delineate the role of circadian clock genes in the anti-fibrotic mechanism of GSS, RNA sequencing (RNA-seq) was conducted on LX-2 cells. The cells were split into the following treatment groups: Control, TGF-β1 (model) and TGF-β1 + GSS (treatment). Analysis of 2,268 genes revealed 817 genes were differentially expressed between the groups (Fig. 4A). Subsequent analysis of the top significantly upregulated and downregulated DEGs across the two comparisons, visualized via radar maps, confirmed that the CLOCK gene was significantly upregulated in the model group compared with the control group. Notably, CLOCK was significantly downregulated in the GSS treatment group compared with the model group; this expression trend was fully consistent with our prior phenotypic observations of CLOCK protein expression

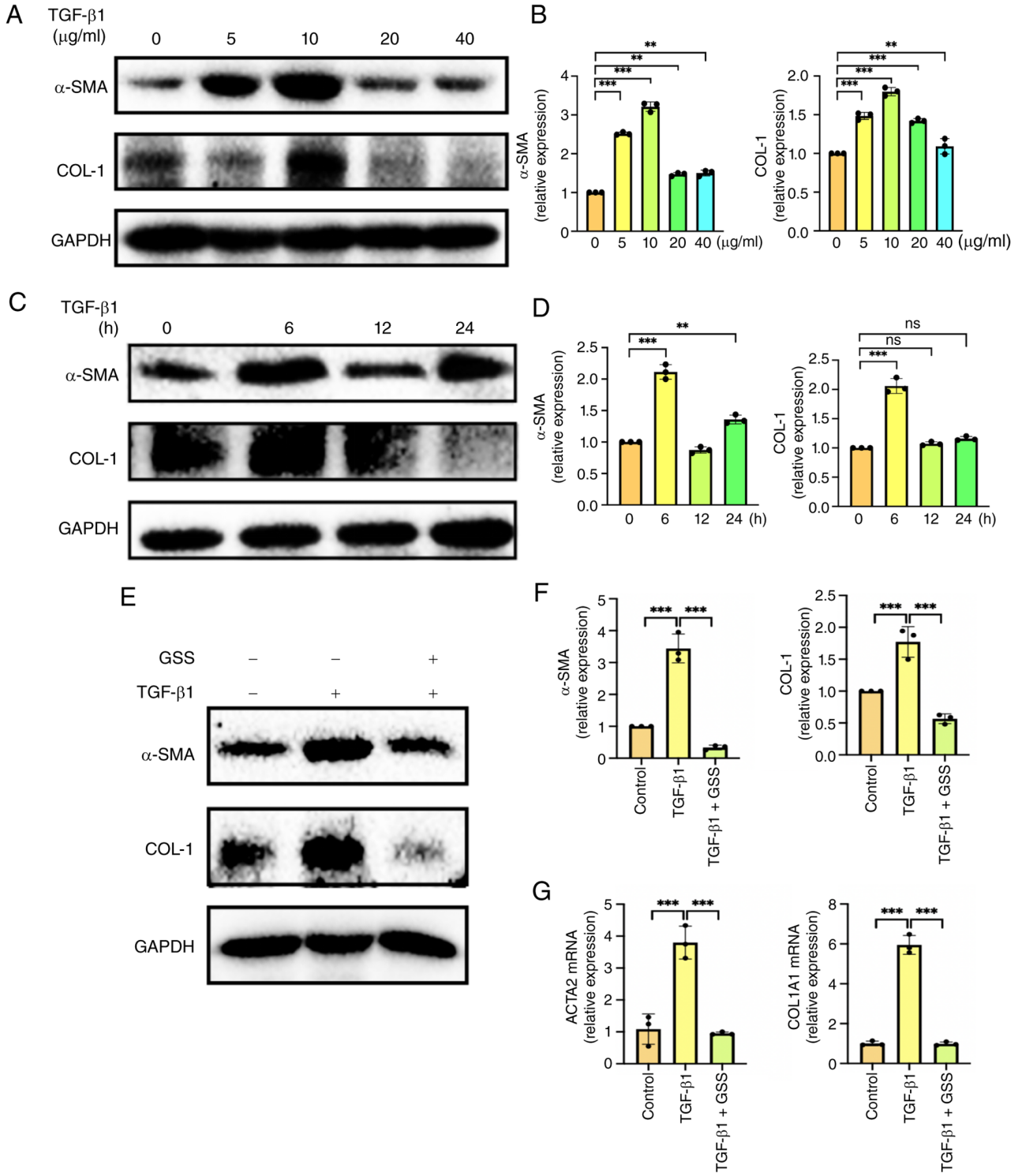

Figure 3. GSS suppresses TGF-β1-induced activation of LX-2 cells. (A) The concentration conditions of TGF-b1-induced cell activation. LX-2 cells were treated with increasing concentrations (0, 5, 10, 20 and 40 μg/ml) of TGF-β1. (B) Dose-dependent expression of α-SMA and COL-1 proteins in TGF-β1-induced cell activation. At a TGF-β1 stimulation concentration of 10 μg/ml, the protein expression of α-SMA and COL-1 was most significant compared with the unstimulated group. (C) Time-course of TGF-b1-induced cell activation. LX-2 cells were treated with 10 μg/ml TGF-β1 for 0, 6, 12 and 24 h. (D) Time-course analysis of α-SMA and COL-1 protein expression in TGF-b1-induced cell activation. Hepatic stellate cell activation was induced by TGF-b1 stimulation at 10 mg/ml for 6 h. (E) Western blot analysis of α-SMA and COL-1 in activated cells. (F) The protein and mRNA expression levels of α-SMA and COL-1 in response to TGF-β1 and GSS treatment. (G) mRNA expression levels of α-SMA and COL-1 in response to TGF-β1 and GSS treatment. Data are presented as the mean ± SD from three independent replicates. **P<0.01, ***P<0.001. α-SMA, α-smooth muscle actin; COL-1, collagen type 1; GSS, ginsenosides; ns, not significant.

in preliminary experiments, which validated the regulatory effect of GSS on CLOCK at the protein level (Fig. 4B). Analysis of the transcriptome by intensive GO analysis showed a significant enrichment of *CLOCK* in 'Circadian rhythm', and the top 10 pathways are shown in Fig. 4C. Kyoto Encyclopedia of Genes and Genomes (KEGG) pathway analysis further

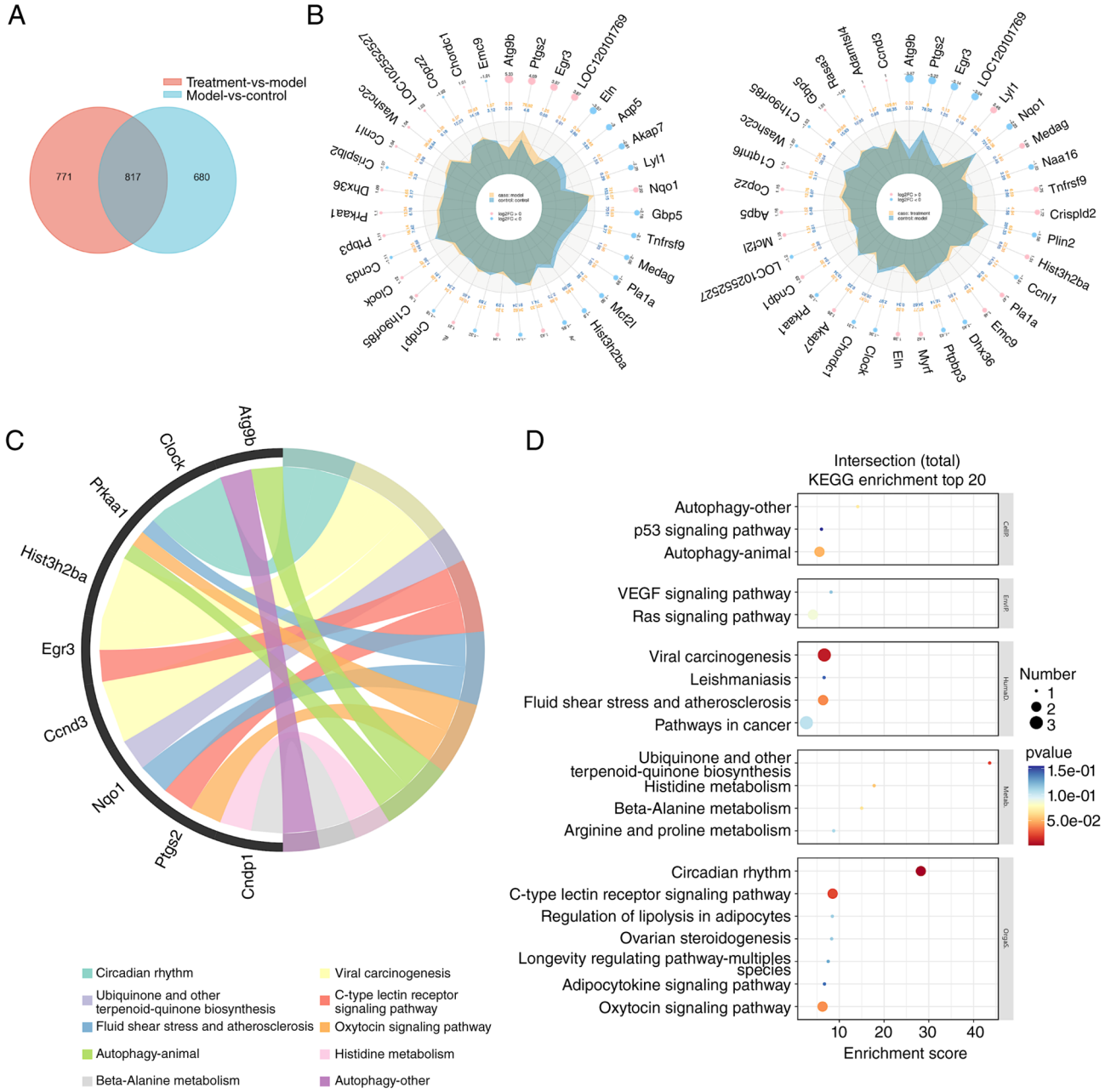

Figure 4. Visualization of RNA-seq results. (A) Differentially expressed gene screening identified a total of 817 genes, the expression of which was significantly dysregulated in the disease model relative to the control group and subsequently restored (fully or partially) following therapeutic intervention. (B) Radar plot of the overlapping circadian clock-associated genes-*CLOCK* genes derived from the RNA-seq comparisons of model vs. control and treatment vs. model groups. (C) KEGG pathway analysis of hepatic fibrosis-associated genes identified by RNA-seq data analysis and (D) bubble plot. KEGG, Kyoto Encyclopedia of Genes and Genomes; RNA-seq, RNA sequencing.

supported this, showing the 'Circadian rhythm' pathway with an enrichment score close to 30, with the size of the bubble indicating a substantial number of associated genes, underscoring its importance in the mechanism of GSS; the top 20 terms are shown in Fig. 4D. The GSEA results for the CLOCK-BMAL1 transcription complex are also presented in the supplementary Fig. S1.

Interaction potential between active constituents of GSS and the core circadian regulator CLOCK. Based on RNA-seq results, CLOCK was shown to be a putative central target for GSS. Molecular docking was subsequently performed to validate interactions between CLOCK and key active constituents of GSS. The CB-Dock2 web server (version 1.0; https://cadd.labshare.cn/cb-dock2/) (26) was employed to as this tool leverages integrated structural models to accurately predict the binding conformation and interaction state of the target CLOCK protein with the input small-molecule ligands. From the mass spectrometry data of GSS performed in the referenced study (27), several major active ingredients of GSS were screened and molecular docking of these active components was performed with the CLOCK protein. Among them, two GSS active ingredients, RB2 and RG5, exhibited high binding affinities, with binding scores of -8.0 kcal/mol

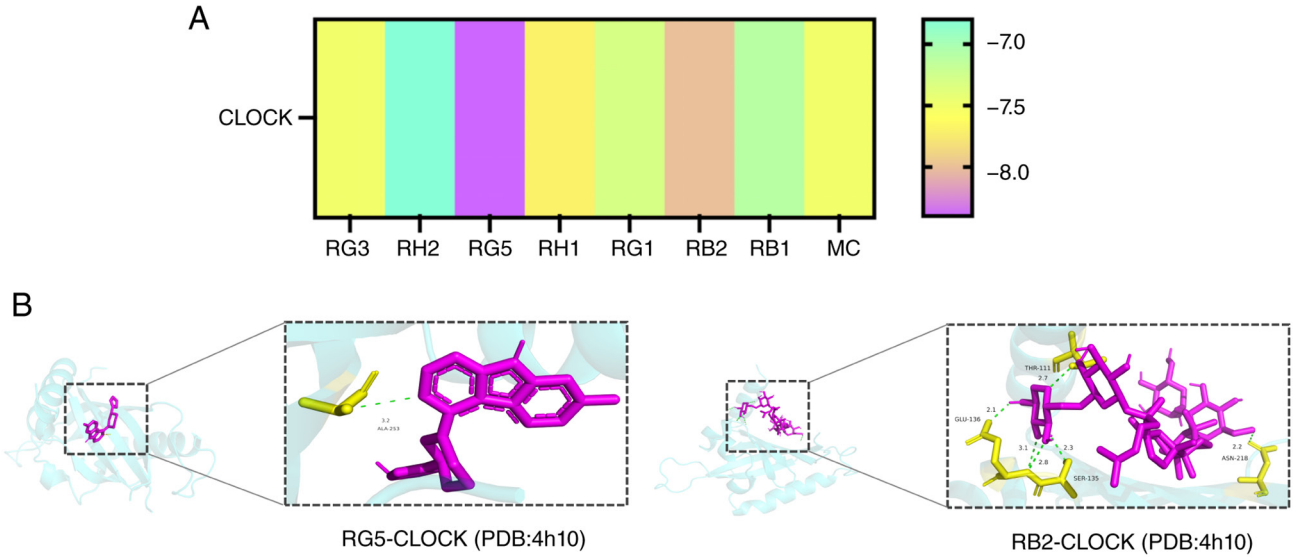

Figure 5. Molecular docking results. (A) Heatmap displaying the predicted binding affinity from molecular docking. (B) Conformations of main active compounds of GSS and the CLOCK protein. *CLOCK*, clock-circadian regulator; GSS, ginsenosides; PDB, Protein Data Bank.

and -8.4 kcal/mol (Fig. 5A and B).The docking results for the remaining six GSS active ingredients with CLOCK are shown in Fig. S2.

GSS modulates circadian clock gene expression in vivo and in vitro. To further investigate alterations in hepatic circadian clock genes during fibrogenesis, the expression levels of these genes in mouse liver samples and cultured cells were evaluated. In CCl_4-induced fibrotic mice, the protein expression of CLOCK, BMAL1 and CRY2 was significantly downregulated, whereas their mRNA expression showed upward trend,both protein and mRNA expression were reversed upon GSS intervention (Fig. 6A and B). The differential expression of circadian clock genes at the protein and mRNA levels reflects the dynamic nature of circadian rhythmic expression. As the peak times of mRNA and protein differ, their expression inevitably exhibits an inherent phase separation. The results of immunohistochemical analysis showed a consistent trend with the pathological staining results of mouse liver (Fig. 6C). Furthermore, it was observed that circadian gene expression was altered in activated HSCs. Previous studies have shown that circadian disorders due to prolonged jet lag or shift work are a direct risk factor for diseases such as obesity and metabolic syndrome, and are associated with increased incidence of non-alcoholic fatty liver disease (NAFLD) (28) and related fibrosis (29). In accordance with this view, the present *in vitro* experiments demonstrated that the protein and mRNA expression levels of CLOCK, BMAL1, CRY1, CRY2 and PER1 was significantly upregulated by TGF-β1, thus indicating HSC activation, whereas they were downregulated by GSS treatment (Fig. 6D-F). These results suggested that the anti-fibrotic effect of GSS may be associated to the correction of circadian disorders.

Role of the CLOCK inhibitor in the anti-fibrotic mechanism of GSS. Building on the findings of the current study (that *CLOCK* is a target gene in the GSS treatment of HF), this role was validated using the CLOCK inhibitor CLK8. CLK8 was administered simultaneously in the control group, the model group (TGF-β1) and the GSS treatment group. The results demonstrated that CLK8 treatment (vs. the TGF-β1 model group) reduced the expression of core circadian genes (including CLOCK, BMAL1 and CRY2) at both the protein and mRNA levels (Fig. 7A and B). However, Compared with the TGF-β1 + GSS group, the TGF-β1 + GSS + CLK8 group showed an upward trend, indicating that the combined use of CLK8 led to a relative increase in the expression of these circadian rhythm genes. Based on the above results, inhibition of Clock expression effectively restores the oscillation of circadian rhythms, maintains circadian clock stability, and significantly suppresses the progression of hepatic fibrosis, this also effectively validated that targeting the clock gene effectively inhibits the development of hepatic fibrosis.

The present study further examined the effect of clock inhibitors on α-SMA protein expression. The experimental results showed that, compared with the TGF-β1 + GSS group, α-SMA protein expression in the TGF-β1 + GSS + CLK8 group exhibited a downward trend, indicating that CLK8 inhibited α-SMA protein expression (Fig. 7C and D). Immunofluorescence analysis confirmed that in HSCs activated by TGF-β1, the phenomenon of enhanced fluorescence intensity of circadian rhythm proteins was weakened after GSS intervention or CLK8 treatment (Fig. 7E).

Discussion

The circadian clock system is an intrinsic timekeeping mechanism capable of harmonizing various physiological processes (30). The positive regulators *BMAL1* and *CLOCK* are at the core of this system and form a heterodimer that activates the transcription of rhythm genes, such as *PER*, *CRY* and *Rev-erbα* (Rev-erbα is encoded by the NR1D1 gene). Subsequently, the negative regulators *PER* and *CRY* accumulate and inhibit *BMAL1*/*CLOCK* activity, creating a feedback loop that drives the oscillating expression of the circadian rhythm-related gene. In the liver, this molecular oscillator

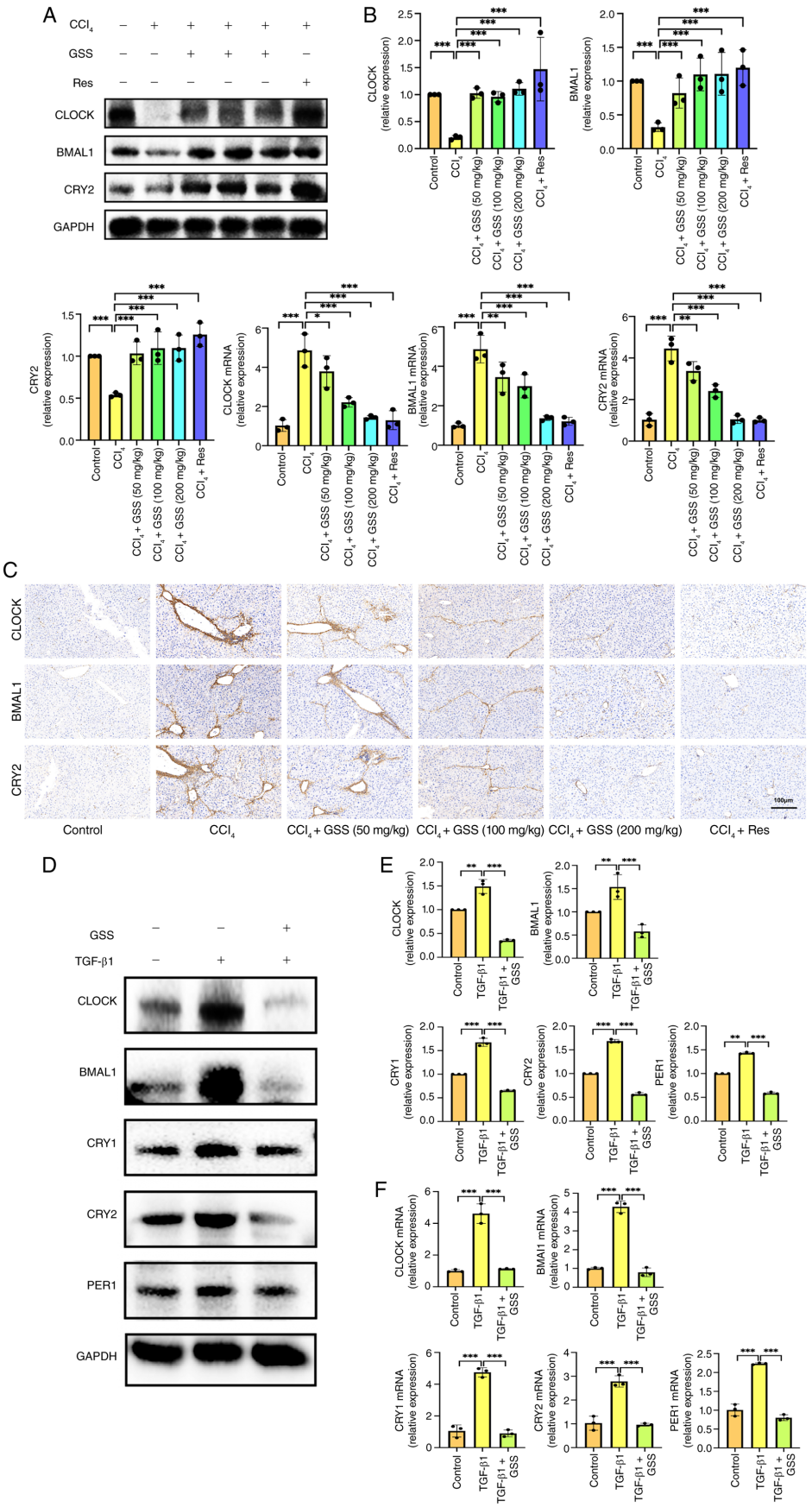

Figure 6. Effects of GSS on circadian clock gene expression in mouse liver samples and in cultured cells. (A) Western blot analysis of the protein levels of key circadian clock genes in mouse liver samples. (B) Statistical analyses of protein expression levels of circadian clock genes in the mouse liver. (C) Immunohistochemical staining of circadian clock proteins in mouse liver tissues. (D) Western blot analysis of the protein levels of key circadian clock genes in LX-2 cells. Statistical analysis of (E) protein and (F) mRNA expression levels of circadian clock genes in LX-2 cells. *P<0.05, **P<0.01, ***P<0.001. BMAL1, basic helix-loop-helix ARNT-like 1; CCl_4, carbon tetrachloride; CLOCK, clock circadian regulator; CRY, cryptochrome; GSS, ginsenosides; PER1, period circadian protein homolog 1; Res, resveratrol.

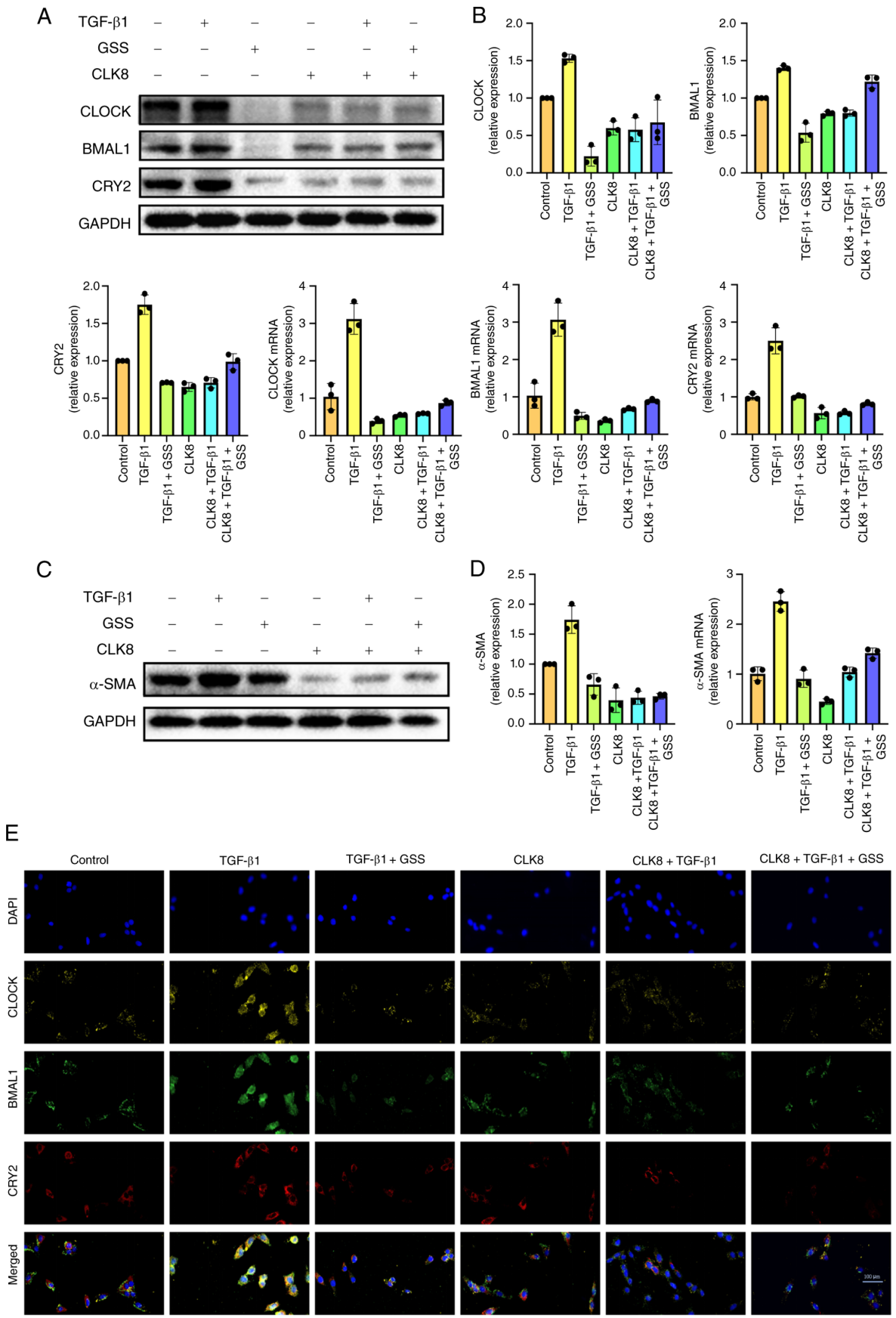

Figure 7. GSS suppresses the progression of liver fibrosis via the clock pathway *in vitro*. (A) Western blot analysis of the protein levels of key circadian clock genes in LX-2 cells after CLOCK pathway inhibition by CLK8. (B) Data are presented as the mean ± SD from three independent replicates. (C) Western blot analysis of the protein levels of α-SMA in LX-2 cells after CLK8 treatment. (D) Statistical analysis of the protein and mRNA levels of α-SMA following CLK8 treatment. Compared with the TGF-β1+GSS group, α-SMA expression was decreased in CLK8-intervention groups. Data are presented as the mean ± SD from three independent replicates. (E) Immunofluorescence analysis of cells following treatment with CLK8. α-SMA, α-smooth muscle actin; BMAL1, basic helix-loop-helix ARNT-like 1; CLOCK, clock circadian regulator; CRY2, cryptochrome 2; GSS, ginsenosides.

serves a central role in maintaining homeostasis of glucose, lipid and bile acid metabolism. The current study demonstrated that the clock gene *CLOCK* serves a critical role in the anti-fibrotic action of GSS. GSS may regulate the circadian rhythm in the mouse liver and could inhibit HF by inhibiting HSCs activation through CLOCK gene targeting, thus supporting the hypothesis that circadian disorders promote HF. These results highlight the importance of circadian regulation in the prevention and treatment of liver disease, including fibrosis.

The precise regulation of circadian rhythms synchronizes hepatic metabolic activities with feeding cycles. For example, the liver prioritizes glycogen synthesis and fat storage during the day, while switching to glyconeogenesis and β-oxidation of fatty acids at night. This disruption of metabolic rate is a key factor in the pathogenesis of chronic liver diseases, including fatty liver disease and fibrosis. Studies have shown that night shifts, sleep deprivation and jet lag may exacerbate the progression of NAFLD to non-alcoholic steatohepatitis (NASH), and even hepatocellular carcinoma, by dysregulating the hepatic circadian transcriptome-metabolome network (31). Numerous investigations have linked circadian disruption to hepatitis, hepatic steatosis, fibrosis and hepatocellular carcinoma. For example, the core clock protein BMAL1 has been shown to regulate mitochondrial dynamics, leading to enhanced oxidative stress and sustained activation of profibrotic TGF-β signaling (32). Furthermore, the Rev-Erbα agonist SR9009 restores liver-gut circadian rhythms, reduces lipopolysaccharide translocation, and ameliorates NASH and early fibrosis (33). *BMAL1* deficiency can disrupt the rhythmic coordination of corticosteroids with insulin, cause systemic insulin resistance and exacerbate diet-induced non-alcoholic steatohepatitis (NASH) (34). A previous 4-year prospective cohort study of 7,236 railway workers found a dose-response relationship between exposure to night work and the incidence of NAFLD (35). Overall, these results highlight the strong link between circadian disorders and the pathogenesis of chronic liver disease. The present study established a mouse model of HF and administered GSS therapeutic intervention. The results demonstrated the effective reversal of fibrosis and the hepatoprotective effects of GSS. GSS significantly reduced serum levels of ALT, AST, ALP, LDH and HF marker levels in model mice, and ameliorated hepatic histopathological alterations. Concurrently, through *in vivo* experimental investigations, circadian rhythm disruption was identified during disease progression in the model mice, and this disruption was gradually reversed following GSS intervention. As natural rhythms are increasingly disrupted by modern lifestyle, targeting circadian rhythms is becoming a promising therapeutic strategy to restore metabolic homeostasis. Therefore, we propose elevating 'circadian disruption' from a associated phenomenon to a modifiable causal factor in liver fibrogenesis, offering a novel paradigm in the interdisciplinary field of circadian, metabolic-inflammatory rhythms, and a circadian treatment strategy for liver disease.

The progression of HF is a coordinated imbalance within multicellular networks, wherein the activation of HSCs is the central driving force. Hematopoietic stem cells, the main effector cells of fibrosis, accelerate the process of fibrosis when their circadian rhythm is disrupted. Under physiological conditions, clock genes in quiescent HSCs help maintain ECM homeostasis by regulating the TGF-β signaling pathway. These quiescent HSCs store vitamin A, and express markers such as glial fibrillary acidic protein and desmin; they also have metabolic regulatory functions, including the secretion of R-spondin 3 to maintain lobular architecture. Upon injury, HSCs rapidly proliferate, migrate and transdifferentiate into myofibroblasts that highly express α-SMA, COL-1 and fibronectin, leading to scar formation (36,37). In biliary injury, portal fibroblasts are activated and act in synergy with the tubular response to cause biliary fibrosis; this process is regulated by multiple signaling networks, of which the TGF-β/Smad pathway forms the core pro-fibrotic axis (37). TGF-β1 signaling directly activates Smad proteins and upregulates fibrogenic genes. In line with this, Chen *et al* (38) demonstrated that targeting the TGF-β/Smad pathway via ECM receptors is capable of inhibiting HSC activation and attenuates fibrosis. In the present study, impaired expression of circadian clock genes in TGF-β1-activated HSCs was observed *in vitro* and circadian disruption in liver tissues from fibrotic mice was confirmed *in vivo*. *In vivo*, compared with the control group, the expression of circadian clock genes Clock, Bmal1, and Cry2 was significantly decreased in the model group mice, which was reversed upon GSS intervention. *In vitro*, the protein expression of circadian clock genes Clock, Bmal1, Cry1, Cry2, and Per1 was significantly increased in the model group cells, and was markedly reversed by GSS treatment. These findings led to the hypothesis that circadian dysregulation may promote HSC activation and HF, a premise for which the underlying mechanisms were subsequently analyzed.

Through RNA-seq, the present study focused on the *CLOCK* gene. The sequencing results revealed that *CLOCK* serves as a target for the anti-fibrotic effects of GSS, and the 'Circadian rhythm' signaling pathway was also identified among the top 20 enriched pathways in KEGG analysis. These sequencing findings were consistent with the observations from *in vivo* and *in vitro* experiments. Furthermore, a CLOCK inhibitor, CLK8, was used for *in vitro* target validation, and the results were consistent with our mechanistic expectation. Treatment with CLK8 alone downregulated α-SMA expression in the TGF-β1-induced fibrotic model group. Moreover, combined intervention with GSS and CLK8 produced a further reduction in α-SMA level relative to GSS single treatment. These findings indicated that pharmacological inhibition of CLOCK augmented the anti-fibrotic capacity of GSS, accompanied by coordinated expression changes of other core circadian clock genes. with concomitant synergistic effects on other circadian clock genes. To the best of our knowledge, Chen *et al* (39) was the first study to reveal a link between the circadian clock and HSC activation; Zhang *et al* (40) further showed that NOX4 is modulated by knock-out of the *BMAL1* gene, resulting in an accumulation of reactive oxygen species (ROS) in the mitochondria. Another study (41) demonstrated substantial dysregulation of hepatic clock genes, particularly *NR1D1*, in a CCl_4-induced murine model; *NR1D1*-deficient mice exhibited greater susceptibility to CCl_4-induced liver fibrosis, supporting its protective effect on fibrogenesis. Notably, the expression patterns of circadian genes in whole mouse liver tissue does not exactly correspond to the results observed in the isolated HSCs. In the present study, CLOCK protein

expression was significantly decreased in the model group in animal experiments; however, it was markedly increased in the TGF-β1-stimulated LX-2 cell model group. These findings indicate that CLOCK displays divergent expression changes under *in vivo* and *in vitro* conditions. Despite this discrepancy, both experimental settings confirm that progression of fibrosis is accompanied by marked circadian disorders. The observed differences are likely attributable to the cellular heterogeneity of liver tissue, where hepatocytes are the majority and may dominate the overall pattern of expression, thus masking the contribution of smaller populations of HSC.

The current study employed RNA transcriptome sequencing to screen and identify CLOCK as a key circadian gene target. In 1994, Vitaterna *et al* (42) identified a heterozygous Clock mutant mouse through N-ethyl-N-nitrosourea (ENU) mutagenesis screening, which exhibited an extended circadian period of approximately 1.1 h. The gene was subsequently cloned and designated as *CLOCK* (42) in 1997 by the laboratories of King and Antoch. The human *CLOCK* gene is situated on chromosome 4q12, spans ~117 kb and comprises 20 exons; its murine ortholog resides on chromosome 5 and exhibits a high degree of structural conservation. The CLOCK protein encompasses several functional domains: bHLH (for DNA binding), PAS-A/B (for protein interaction) and Q-rich (for transcriptional activation), and forms a heterodimer with BMAL1 to bind E-box elements (CACGTG), thus initiating the transcription of the target genes of the rhythm regulation. A study published in 2025 in Nature Neuroscience reported persistently elevated, non-circadian expression of *CLOCK* in the human neocortex; humanized CLOCK knock-in mice showed long-term improved hippocampal synaptic plasticity and 30% improved spatial memory capacity. These phenotypes, which are independent of circadian rhythmicity, suggesting that the *CLOCK* acquired new functions novel neurodevelopmental functions during human brain evolution, likely mediated by its sustained cortical expression and enhanced synaptic protein interactions (43). Lu *et al* proposed that *CLOCK* knockdown can suppress the differentiation of mouse induced pluripotent stem cells (iPSCs) into the three germ layers while sustaining high Oct4/Sox2 expression, indicating a role for the circadian clock in regulating the exit from pluripotency and guiding iPSC differentiation (44). In metabolic studies, *CLOCK*$^{\Delta}$19 mutant mice have been reported to develop obesity and hyperlipidemia (45), and the human 3111T/C polymorphism has been associated with night-eating behavior and increased BMI (46). Subsequently, the CLOCK-specific inhibitor CLK8 was utilized in the current study to examine the suppression of this predicted target gene on markers of liver fibrosis, as well as the expression of other circadian genes. The results demonstrated that compared with the GSS treatment alone group, the GSS treatment group with CLOCK inhibitor intervention showed a decrease expression of the fibrotic marker α-SMA, indicating a stronger therapeutic efficacy of the pharmacological intervention. This is further evidence that *CLOCK* is a promising therapeutic target.

Currently, there is a substantial body of research on GSS for the treatment of HF. The primary active extracts from *Panax* plants contain >20 monomeric saponins, among which Rg1 (47), Rd (48), Rh1 and Rh2 (49) have been proven to exert notable hepatoprotective effects. The effects of GSS on liver protection, enzyme reduction, anti-inflammatory activity and antioxidant capacity have been extensively investigated. As the principal active component of the traditional Chinese medicine ginseng, GSS exhibits multi-target effects in anti-fibrotic therapies. For example, GSS (primarily containing Rb1 and Rg1) can inhibit HSC activation, downregulate α-SMA and COL1A1 protein expression in LX-2 cells at concentrations of 10-40 μg/ml, and reduce ROS stimulated by platelet-derived growth factor (50). Li *et al* (51) utilized GSS to alleviate liver inflammation and impede the progression from fibrosis to cirrhosis. Yang *et al* (52) employed data mining to elucidate and validate the mechanisms through which GSS ameliorates alcoholic hepatitis. Although, to the best of our knowledge, there are no reports on the direct interaction between GSS and circadian clock genes, studies have indicated that GSS reduces ROS via the Nrf2 signaling pathway and ROS has been proven to disrupt *BMAL1*/*CLOCK* oscillations (53), suggesting that its anti-fibrotic effects may be partially related to the restoration of redox rhythms. Furthermore, ginsenoside Rb1 (54) has been shown to synchronize hepatic lipid metabolic rhythms in a high-fat diet model by activating AMPK phosphorylation and upregulating the circadian expression of PPAR-α and SREBP-1c. Additionally, it can improve diurnal fluctuations in lipid metabolism by modulating AMPK phosphorylation, in parallel with the rhythm of *CLOCK*-regulated SREBP-1c. These findings imply a potential direct connection between GSS and circadian clock genes. The current study directly applied GSS to mice with CCl_4-induced fibrosis and to activated HSCs. The results demonstrated that GSS may effectively reverse liver fibrosis and modulate circadian rhythms, which is consistent with the initial hypothesis.

In recent years, traditional Chinese medicine has been reported to serve an increasingly notable role in the field of anti-fibrosis treatment, with an expanding number of traditional Chinese medicine monomers and compound formulas being incorporated into clinical practice. For example, salvianolic acid B, a major water-soluble active monomer isolated from Salvia miltiorrhiza Bge., has been extensively confirmed to exert significant anti-fibrotic effects in various fibrotic diseases, such as alleviating hepatic fibrosis by targeting PDGFRβ to inhibit hepatic stellate cell activation and proliferation (55). Another classic TCM monomer, astragaloside IV from Astragalus mongholicus Bunge., can relieve liver, renal and cardiac fibrosis by suppressing the TGF-β1/Smad signaling pathway and inhibiting epithelial-mesenchymal transition (56). The hepatoprotective and anti-HF effects of GSS have been extensively investigated; however, their underlying mechanisms still require substantial research support. The present study focused on the adverse effects of the hepatic circadian clock on HF. Following the observation of global alterations in circadian clock gene expression, an inhibitor targeting the CLOCK protein was employed to validate the findings through suppression of target gene expression. The results demonstrated that inhibition of CLOCK expression effectively ameliorated circadian rhythm disruption and suppressed the progression of HF. Therefore, based on these experimental findings, it may be concluded that GSS targets the *CLOCK* gene to regulate circadian rhythm, thus ameliorating the development of HF.

Acknowledgements

Not applicable.

Funding

The present study was financially supported by the National Natural Science Foundation of China Project (grant no. 82204816).

Availability of data and materials

The RNA-seq data generated in the present study may be found in the NCBI Sequence Read Archive under accession number PRJNA1436159 or at the following URL: https://www.ncbi.nlm.nih.gov/bioproject/PRJNA1436159. The other data generated in this study are available from the corresponding author upon request.

Authors' contributions

RQ conceived and designed the experiments. YZ designed the experimental framework for this study and proposed the core hypotheses, revised the manuscript, provided guiding suggestions and approved the final version of the manuscript for publication. CQ acquired, analyzed and interpreted working data and experimental results. JY performed the experiments, analyzed the data and wrote the manuscript. YZ and CQ confirm the authenticity of all the raw data. All authors read and approved the final manuscript.

Ethics approval and consent to participate

All procedures conformed to National Standards for Laboratory Animals of China and were approved by the Animal Ethics and Welfare Committee of Shanghai Municipal Hospital of Traditional Chinese Medicine (ethics approval no. 2025051; Shanghai, China).

Patient consent for publication

Not applicable.

Competing interests

The authors declare that they have no competing interests.

References

1. Roehlen N, Crouchet E and Baumert TF: Liver fibrosis: Mechanistic concepts and therapeutic perspectives. Cells 9: 875, 2020.
2. De Siervi S, Cannito S and Turato C: Chronic liver disease: Latest research in pathogenesis, detection and treatment. Int J Mol Sci 24: 10633, 2023.
3. Kisseleva T and Brenner D: Molecular and cellular mechanisms of liver fibrosis and its regression. Nat Rev Gastroenterol Hepatol 18: 151-166, 2021.
4. Tsuchida T and Friedman SL: Mechanisms of hepatic stellate cell activation. Nat Rev Gastroenterol Hepatol 14: 397-411, 2017.
5. Yu Q: Biological clock: The oscillator of gene expression. Sci China Life Sci 61: 128-130, 2018.
6. Brooks JF II and Hooper LV: Interactions among microbes, the immune system, and the circadian clock. Semin Immunopathol 42: 697-708, 2020.
7. Richards J and Gumz ML: Advances in understanding the peripheral circadian clocks. FASEB J 26: 3602-3613, 2012.
8. Bolshette N, Ibrahim H, Reinke H and Asher G: Circadian regulation of liver function: From molecular mechanisms to disease pathophysiology. Nat Rev Gastroenterol Hepatol 20: 695-707, 2023.
9. Mukherji A, Bailey SM, Staels B and Baumert TF: The circadian clock and liver function in health and disease. J Hepatol 71: 200-211, 2019.
10. Farshadi E, van der Horst GTJ and Chaves I: Molecular links between the circadian clock and the cell cycle. J Mol Biol 432: 3515-3524, 2020.
11. Skrlec I and Talapko J: Hepatitis B and circadian rhythm of the liver. World J Gastroenterol 28: 3282-3296, 2022.
12. Frazier K, Manzoor S, Carroll K, DeLeon O, Miyoshi S, Miyoshi J, St George M, Tan A, Chrisler EA, Izumo M, *et al*: Gut microbes and the liver circadian clock partition glucose and lipid metabolism. J Clin Invest 133: e162515, 2023.
13. Crouchet E, Dachraoui M, Jühling F, Roehlen N, Oudot MA, Durand SC, Ponsolles C, Gadenne C, Meiss-Heydmann L, Moehlin J, *et al*: Targeting the liver clock improves fibrosis by restoring TGF-β signaling. J Hepatol 82: 120-133, 2025.
14. Mawatari K, Koike N, Nohara K, Wirianto M, Uebanso T, Shimohata T, Shikishima Y, Miura H, Nii Y, Burish MJ, *et al*: The polymethoxyflavone sudachitin modulates the circadian clock and improves liver physiology. Mol Nutr Food Res 67: e2200270, 2023.
15. Radi SH, Vemuri K, Martinez-Lomeli J and Sladek FM: HNF4α isoforms: The fraternal twin master regulators of liver function. Front Endocrinol (Lausanne) 14: 1226173, 2023.
16. Rashed N, Liu W, Zhou X, Bode AM and Luo X: The role of circadian gene CLOCK in cancer. Biochim Biophys Acta Mol Cell Res 1871: 119782, 2024.
17. Boiko DI, Chopra H, Bilal M, Kydon PV, Herasymenko LO, Rud VO, Bodnar LA, Vasylyeva GY, Isakov RI, Zhyvotovska LV, *et al*: Schizophrenia and disruption of circadian rhythms: An overview of genetic, metabolic and clinical signs. Schizophr Res 264: 58-70, 2024.
18. Kettner NM, Voicu H, Finegold MJ, Coarfa C, Sreekumar A, Putluri N, Katchy CA, Lee C, Moore DD and Fu L: Circadian homeostasis of liver metabolism suppresses hepatocarcinogenesis. Cancer Cell 30: 909-924, 2016.
19. Li J, Zhao J, Wang X, Lin Z, Lin H and Lin Z: Ginsenoside-a promising natural active ingredient with steroidal hormone activity. Food Funct 15: 1825-1839, 2024.
20. Hu Y, Lang Z, Li X, Lin L, Li Y, Zhang R, Zheng J and Yu Z: Ginsenoside Rg3 promotes hepatic stellate cell ferroptosis by epigenetically regulating ACSL4 to suppress liver fibrosis progression. Phytomedicine 124: 155289, 2024.
21. Liu X, Mi X, Wang Z, Zhang M, Hou J, Jiang S, Wang Y, Chen C and Li W: Ginsenoside Rg3 promotes regression from hepatic fibrosis through reducing inflammation-mediated autophagy signaling pathway. Cell Death Dis 11: 454, 2020.
22. Zhou H, Liu Y, Su Y, Ji P, Kong L, Sun R, Zhang D, Xu H, Li W and Li W: Ginsenoside Rg1 attenuates lipopolysaccharide-induced chronic liver damage by activating Nrf2 signaling and inhibiting inflammasomes in hepatic cells. J Ethnopharmacol 324: 117794, 2024.
23. Zhang K, Li J, Shi Z, Zhu Y, Yang J, Liu X, Que R, Lin L, Chen Y and Li Y: Ginsenosides regulates innate immunity to affect immune microenvironment of AIH through hippo-YAP/TAZ signaling pathway. Front Immunol 13: 851560, 2022.
24. Livak KJ and Schmittgen TD: Analysis of relative gene expression data using real-time quantitative PCR and the 2(-Delta Delta C(T)) method. Methods 25: 402-408, 2001.
25. Luo L, Wang S, Du R, Zhong M, Zhu W, Huang F, Ouyang W, Huang J and Tong G: HBHP ameliorates CCL4-induced liver fibrosis in rats by inhibiting HMGB1-mediated inflammatory response through binding to the HMGB1-A box. Eur J Pharmacol 1004: 177971, 2025.
26. Liu Y, Yang X, Gan J, Chen S, Xiao ZX and Cao Y: CB-Dock2: Improved protein-ligand blind docking by integrating cavity detection, docking and homologous template fitting. Nucleic Acids Res 50 (W1): W159-W164, 2022.
27. Li ZY, Dai YX, Wu ZM, Li G, Pu PM, Hu CW, Zhou LY, Zhu K, Shu B, Wang YJ, *et al*: Network pharmacology analysis and animal experiment validation of neuroinflammation inhibition by total ginsenoside in treating CSM. Phytomedicine 126: 155073, 2024.
28. Zheng R, Xiang X, Shi Y, Qiu A, Luo X, Xie J, Russell R and Zhang D: Chronic jet lag alters gut microbiome and mycobiome and promotes the progression of MAFLD in HFHFD-fed mice. Front Microbiol 14: 1295869, 2023.

29. Arab A, Karimi E, Garaulet M and Scheer FAJL: Social jetlag and obesity: A systematic review and meta-analysis. Obes Rev 25: e13664, 2024.
30. Zhang R, Lahens NF, Ballance HI, Hughes ME and Hogenesch JB: A circadian gene expression atlas in mammals: Implications for biology and medicine. Proc Natl Acad Sci USA 111: 16219-16224, 2014.
31. Singh A, Anjum B, Naz Q, Raza S, Sinha RA, Ahmad MK, Mehdi AA and Verma N: Night shift-induced circadian disruption: Links to initiation of non-alcoholic fatty liver disease/non-alcoholic steatohepatitis and risk of hepatic cancer. Hepatoma Res 10: 88, 2024.
32. Peng D, Fu M, Wang M, Wei Y and Wei X: Targeting TGF-β signal transduction for fibrosis and cancer therapy. Mol Cancer 21: 104, 2022.
33. Ni Y, Zhao Y, Ma L, Wang Z, Ni L, Hu L and Fu Z: Pharmacological activation of REV-ERBα improves nonalcoholic steatohepatitis by regulating intestinal permeability. Metabolism 114: 154409, 2021.
34. Jouffe C, Weger BD, Martin E, Atger F, Weger M, Gobet C, Ramnath D, Charpagne A, Morin-Rivron D, Powell EE, *et al*: Disruption of the circadian clock component BMAL1 elicits an endocrine adaption impacting on insulin sensitivity and liver disease. Proc Natl Acad Sci USA 119: e2200083119, 2022.
35. Xu J, Ni S, Wang Y, Yan M, Yang X, Ge H, Jia Z, Yang Z, Shan A, Liu H and Tang NJ: Shift work and nonalcoholic fatty liver disease incidence among Chinese rail workers: A 4-year longitudinal cohort study. Int Arch Occup Environ Health 96: 179-190, 2023.
36. Jokl E, Llewellyn J, Simpson K, Adegboye O, Pritchett J, Zeef L, Donaldson I, Athwal VS, Purssell H, Street O, *et al*: Circadian disruption primes myofibroblasts for accelerated activation as a mechanism underpinning fibrotic progression in non-alcoholic fatty liver disease. Cells 12: 1582, 2023.
37. Hu HH, Chen DQ, Wang YN, Feng YL, Cao G, Vaziri ND and Zhao YY: New insights into TGF-β/Smad signaling in tissue fibrosis. Chem Biol Interact 292: 76-83, 2018.
38. Chen C, Chen J, Wang Y, Fang L, Guo C, Sang T, Peng H, Zhao Q, Chen S, Lin X and Wang X: Ganoderma lucidum polysaccharide inhibits HSC activation and liver fibrosis via targeting inflammation, apoptosis, cell cycle, and ECM-receptor interaction mediated by TGF-β/Smad signaling. Phytomedicine 110: 154626, 2023.
39. Chen P, Kakan X and Zhang J: Altered circadian rhythm of the clock genes in fibrotic livers induced by carbon tetrachloride. FEBS Lett 584: 1597-1601, 2010.
40. Zhang D, Tong X, Arthurs B, Guha A, Rui L, Kamath A, Inoki K and Yin L: Liver clock protein BMAL1 promotes de novo lipogenesis through insulin-mTORC2-AKT signaling. J Biol Chem 289: 25925-25935, 2014.
41. Chen L, Xia S, Wang F, Zhou Y, Wang S, Yang T, Li Y, Xu M, Zhou Y, Kong D, *et al*: m^{6}A methylation-induced NR1D1 ablation disrupts the HSC circadian clock and promotes hepatic fibrosis. Pharmacol Res 189: 106704, 2023.
42. Vitaterna MH, King DP, Chang AM, Kornhauser JM, Lowrey PL, McDonald JD, Dove WF, Pinto LH, Turek FW and Takahashi JS: Mutagenesis and mapping of a mouse gene, Clock, essential for circadian behavior. Science 264: 719-725, 1994.
43. Sun Y, Shui K, Li Q, Liu C, Jin W, Ni JQ, Lu J and Zhang L: Upstream open reading frames dynamically modulate CLOCK protein translation to regulate circadian rhythms and sleep. PLoS Biol 23: e3003173, 2025.
44. Lu C, Yang Y, Zhao R, Hua B, Xu C, Yan Z, Sun N and Qian R: Role of circadian gene Clock during differentiation of mouse pluripotent stem cells. Protein Cell 7: 820-832, 2016.
45. Turek FW, Joshu C, Kohsaka A, Lin E, Ivanova G, McDearmon E, Laposky A, Losee-Olson S, Easton A, Jensen DR, *et al*: Obesity and metabolic syndrome in circadian Clock mutant mice. Science 308: 1043-1045, 2005.
46. Monteleone P, Tortorella A, Docimo L, Maldonato MN, Canestrelli B, De Luca L and Maj M: Investigation of 3111T/C polymorphism of the CLOCK gene in obese individuals with or without binge eating disorder: Association with higher body mass index. Neurosci Lett 435: 30-33, 2008.
47. Gao Q, Li G, Zu Y, Xu Y, Wang C, Xiang D, He W, Shang T, Cheng X, Liu D and Zhang C: Ginsenoside Rg1 alleviates ANIT-induced cholestatic liver injury by inhibiting hepatic inflammation and oxidative stress via SIRT1 activation. J Ethnopharmacol 319: 117089, 2024.
48. Yang X, Gao M, Miao M, Jiang C, Zhang D, Yin Z, Ni Y, Chen J and Zhang J: Combining combretastatin A4 phosphate with ginsenoside Rd synergistically inhibited hepatocellular carcinoma by reducing HIF-1α via PI3K/AKT/mTOR signalling pathway. J Pharm Pharmacol 73: 263-271, 2021.
49. Chen X, Yang S, Nan B, Ma J and Wang Y: Mechanisms of the anti-fibrotic effect of ginsenoside Rh_1 on hepatic fibrosis. Sichuan Da Xue Xue Bao Yi Xue Ban 56: 120-128, 2025 (In Chinese).
50. Jiang L, Yin X, Chen YH, Chen Y, Jiang W, Zheng H, Huang FQ, Liu B, Zhou W, Qi LW and Li J: Proteomic analysis reveals ginsenoside Rb1 attenuates myocardial ischemia/reperfusion injury through inhibiting ROS production from mitochondrial complex I. Theranostics 11: 1703-1720, 2021.
51. Li N, Zhu C, Fu R, Ma X, Duan Z and Fan D: Ginsenoside Rg5 inhibits lipid accumulation and hepatocyte apoptosis via the Notch1 signaling pathway in NASH mice. Phytomedicine 124: 155287, 2024.
52. Yang C, He X, Zhao J and Huang W: Hepatoprotection by ginsenoside Rg1 in alcoholic liver disease. Int Immunopharmacol 92: 107327, 2021.
53. Jin W, Li C, Yang S, Song S, Hou W, Song Y and Du Q: Hypolipidemic effect and molecular mechanism of ginsenosides: A review based on oxidative stress. Front Pharmacol 14: 1166898, 2023.
54. Gao Y, Chu S, Zhang Z and Chen N: Hepataprotective effects of ginsenoside Rg1-A review. J Ethnopharmacol 206: 178-183, 2017.
55. Liu F, Li S, Chen P, Gu Y, Wang S, Wang L, Chen C, Wang R and Yuan Y: Salvianolic acid B inhibits hepatic stellate cell activation and liver fibrosis by targeting PDGFRβ. Int Immunopharmacol 122: 110550, 2023.
56. Wu M, Li K, Wu J, Zhang Q, Ma X, Dai W, Gao H, Ding X, Wang W and Xiao W: Astragaloside IV: A multipotent phytochemical for treating fibrotic diseases (review). Int J Mol Med 57: 50, 2026.